ZBTB7A promotes malignant phenotypes in ovarian cancer through transcriptional activation of CRLF1

XIAOBAI HAO[1,2] and YU CHEN[1]

[1]Department of Obstetrics and Gynecology, The First Affiliated Hospital of Naval Medical University, Shanghai 200433, P.R. China; [2]Department of Obstetrics and Gynecology, The Seventh People's Hospital of Shanghai University of Traditional Chinese Medicine, Shanghai 200137, P.R. China

Received October 9, 2025; Accepted January 30, 2026

DOI: 10.3892/or.2026.9107

Abstract. Ovarian cancer (OV) remains the most lethal gynecological malignancy, owing to late-stage diagnosis, high metastatic potential and limited therapeutic efficacy. Although the transcription factor zinc finger and BTB domain-containing 7A (ZBTB7A) has been implicated in several types of cancer, its role in OV has not yet been systematically characterized. The present study comprehensively investigated the expression pattern, prognostic relevance, functional role and downstream mechanisms of ZBTB7A in OV progression. Multi-cohort transcriptomic analyses across independent public datasets revealed consistent upregulation of ZBTB7A in OV tissues, and high expression predicted a significantly poor prognosis. Single-cell RNA sequencing demonstrated that ZBTB7A-high tumor cells were enriched in proliferative, migratory and epithelial-mesenchymal transition-related programs, accompanied by activation of oncogenic pathways such as Wnt/β-catenin and Hippo-YAP. Functional assays using overexpression and RNA interference demonstrated that ZBTB7A enhanced malignant phenotypes, including increased cell proliferation, DNA synthesis, clonogenic survival and migration. Further analyses identified cytokine receptor-like factor 1 (CRLF1) as a key downstream effector of ZBTB7A. ZBTB7A overexpression elevated CRLF1 transcription, whereas CRLF1 knockdown abrogated ZBTB7A-induced proliferation and migration, defining a functional ZBTB7A/CRLF1 oncogenic axis. Collectively, these findings establish ZBTB7A as an important transcriptional driver of OV aggressiveness and highlight the ZBTB7A/CRLF1 regulatory pathway as a potential prognostic biomarker and therapeutic target.

Correspondence to: Professor Yu Chen, Department of Obstetrics and Gynecology, The First Affiliated Hospital of Naval Medical University, 168 Changhai Road, Shanghai 200433, P.R. China
E-mail: cheny2979@163.com

Key words: ovarian cancer, zinc finger and BTB domain-containing 7A, cytokine receptor-like factor 1, single-cell RNA sequencing, transcriptional activation

Introduction

Ovarian cancer (OV) is the leading cause of mortality among gynecological malignancies worldwide (1,2). Despite progress in cytoreductive surgery, chemotherapy and targeted therapies, the overall 5-year survival rate remains low, at 45-50% across all stages, particularly among patients who present with advanced-stage disease (3-5). A major limitation in improving patient outcomes is the absence of reliable biomarkers and actionable molecular targets that can aid early detection, guide treatment selection or predict prognosis (6,7). Consequently, there is a need to elucidate the transcriptional programs that drive OV initiation, progression and therapeutic resistance.

Transcription factors (TFs) are key regulators of gene expression networks governing cell proliferation (8,9), epithelial-mesenchymal transition (EMT) (10,11), invasion (12,13) and stress adaptation (14). Aberrant TF activity is implicated in the pathogenesis of numerous malignancies (15), where TFs often reprogram cellular states to sustain tumor growth and dissemination; for example, in ovarian cancer, the lineage TF PAX8 cooperates with MECOM/PRDM3 to drive oncogenic transcriptional programs and sustain *in vivo* tumor growth (16). However, in OV, TF-driven oncogenic circuits have undergone comparatively less systematic investigation than alterations in signaling pathways or genetic mutations (17,18). Identifying TFs that are consistently dysregulated and defining downstream targets may provide novel insights into and uncover previously unrecognized therapeutic vulnerabilities.

Zinc finger and BTB domain-containing 7A (ZBTB7A, also known as LRF or Pokemon) is a member of the POK family of transcriptional regulators (19-21). ZBTB7A has been reported to function as either an oncogene or a tumor suppressor in a context-dependent manner (21). In some cancers, ZBTB7A enhances proliferation, metabolic adaptation and resistance to apoptosis, whereas in others it appears to constrain tumorigenesis (22). Despite these diverse roles, the relevance of ZBTB7A in OV has remained largely unexplored. To date, to the best of our knowledge, there has been little evidence addressing whether ZBTB7A contributes to ovarian tumor progression (23), what downstream transcriptional programs it engages, and whether these programs have prognostic or therapeutic importance.

The present study aimed to investigate the role of ZBTB7A in OV. Specifically, the current study assessed the clinical relevance of ZBTB7A in OV and aimed to delineate the molecular circuitry through which ZBTB7A may promote malignant phenotypes, including the investigation of cytokine receptor-like factor 1 (CRLF1) as a candidate downstream effector.

Materials and methods

Gene Expression Omnibus (GEO) datasets and differential expression analysis. Public gene expression profiles were retrieved from four GEO datasets (https://www.ncbi.nlm.nih.gov/geo): GSE26712 (24), GSE160626, GSE143897 (25) and GSE119168 (26). Briefly, GSE26712 is an Affymetrix microarray cohort consisting of primary ovarian tumor specimens from patients (late-stage, high-grade disease) and healthy controls. GSE160626 is an RNA sequencing (RNA-seq) cohort comparing platinum-sensitive and platinum-resistant ovarian cancer cases, which also includes 'normal ovary' samples; however, the GEO metadata does not specify whether these normal samples were obtained from healthy donors or from the non-malignant (adjacent) tissues of patients. GSE143897 is an RNA-seq dataset of patient-derived ovarian cancer samples (primary tumors, ascites and post-treatment tissues) and was used accordingly (not as a strict tumor-vs.-normal ovary comparison). GSE119168 includes patient-derived high-grade serous ovarian cancer omental tumor tissues and non-malignant controls, which were normal fallopian tube tissues from patients with benign gynecological conditions. Datasets included both ovarian tumor and normal ovarian tissue samples (n=309), with GSE26712 containing 176 sample (OV=166 and normal controls=10), GSE160626 containing 17 sample (OV=9 and normal controls=8), GSE143897 containing 90 sample (OV=78 and normal controls=12) and GSE119168 containing 26 sample (OV=12 and normal controls=14).

Raw expression matrices were downloaded and processed in R (version 4.5.2; https://www.r-project.org/). Differential expression analysis was performed using the Bioconductor packages GEOquery (version 2.78.0; https://bioconductor.org/packages/release/bioc/html/GEOquery.html) and limma (version 3.66.0; https://bioconductor.org/packages/release/bioc/html/limma.html). GEOquery was used to programmatically retrieve GEO data, and limma was used for linear modeling and differential expression testing. Differentially expressed genes (DEGs) were identified using thresholds of adjusted $P<0.05$ and $|\log_2$ fold change$|>1$. Overlapping DEGs across datasets were visualized by Venn diagrams and representative volcano plots, which were created using the ggplot2 package (version 3.4.4; https://cran.r-project.org/package=ggplot2) in R (version stated above; Bioconductor release 3.22). In addition, ZBTB7A and CRLF1 pan-cancer expression was retrieved from TNMplot (https://tnmplot.com/), using its pan-cancer RNA-seq module integrating The Cancer Genome Atlas (TCGA) data; the tumor and tissue-matched healthy samples were provided by the TNMplot pipeline, in which normal tissues are automatically matched to tumor types according to tissue of origin and anatomical annotation. Statistical comparisons were performed using the Mann-Whitney U test implemented in TNMplot. Kaplan-Meier overall survival (OS) analysis was performed in Gene Expression Profiling Interactive Analysis (GEPIA; http://gepia.cancer-pku.cn/) based on TCGA-OV RNA-seq data, using median expression as the cut-off (high vs. low, 50/50%) and the log-rank test to assess significance. Correlation analyses between ZBTB7A and candidate target genes were performed using the Pearson correlation coefficient based on transcriptomic data from TCGA-OV cohort (GEPIA).

Survival and Cox regression analyses. OS time was defined as the interval from the date of initial diagnosis to death or last follow-up; patients alive at the last follow-up were censored. OS data were obtained from TCGA-OV dataset (n=379 patients). Expression levels of ZBTB7A and CRLF1 were dichotomized into high and low groups according to the median mRNA expression value. Age was treated as a continuous variable. Tumor grade was dichotomized into low grade (G1-G2) and high grade (G3-G4, borderline grade and grade could not be assessed). Univariate Cox proportional hazards models were first used to estimate hazard ratios (HRs) and 95% confidence intervals (CIs) for ZBTB7A and CRLF1. Multivariate Cox models were then constructed to assess whether ZBTB7A and CRLF1 were independent prognostic factors, adjusting for age and tumor grade, which were included *a priori* as clinically established prognostic covariates to control for potential confounding effects irrespective of their univariate significance. Stage information was not available for the majority of cases in TCGA-OV dataset and therefore could not be included as a covariate. All analyses were performed using R (version 4.5.2) or Python (version 3.11; Python Software Foundation; https://www.python.org/) and two-sided $P<0.05$ was considered to indicate a statistically significant difference.

Human Protein Atlas (HPA). Protein expression data were obtained from the HPA (https://www.proteinatlas.org/). Immunohistochemistry images of ZBTB7A in normal ovary tissues and ovarian cancer tissues were retrieved from HPA.

Single-cell RNA-seq analysis. Single-cell transcriptomic data from OV samples were obtained from the GEO (GSE154600) (27). According to the original publication, the dataset consists of 10X Genomics single-cell RNA sequencing from five cases of high-grade serous ovarian carcinoma (HGSOC), yielding a total of 42,000 tumor-associated cells. These samples represent infiltrated HGSOC with extensive genomic instability and heterogeneous tumor microenvironment composition. Raw count matrices were processed using Seurat (v4.3) in R (https://satijalab.org/seurat/; https://github.com/satijalab/seurat). Cells were subjected to standard quality control filtering; specifically, cells expressing <200 genes or >6,000 genes were excluded to remove low-quality cells and potential doublets. In addition, cells with mitochondrial gene content >10% were removed. Genes detected in <3 cells were excluded from downstream analyses. After quality control, the filtered gene expression matrix was normalized using the LogNormalize method with a scaling factor of 10,000. Cells were filtered for quality control, normalized and subjected to principal component analysis using RunPCA (implemented in Seurat and relying on standard R routines for singular

value decomposition). Specifically, RunUMAP (UMAP), FindNeighbors and FindClusters in Seurat package v4.3.0 in R were used for dimensionality reduction and cluster identification. Module scoring was performed using AddModuleScore (Seurat package v4.3.0 in R version 4.5.2) function to calculate EMT scores based on the Molecular Signatures Database (MSigDB) HALLMARK_EPITHELIAL_MESENCHYMAL_TRANSITION gene set; migration score using a curated migration gene signature including VIM, FN1, ITGA5, ITGB1, MMP2, MMP9 and CXCL8; and proliferation score using the MSigDB HALLMARK_G2M_CHECKPOINT and HALLMARK_E2F_TARGETS gene sets. These Hallmark gene sets were obtained from the Human MSigDB v2025.1.Hs https://www.gsea-msigdb.org/gsea/msigdb). Tumor epithelial cells were stratified into ZBTB7A-high and ZBTB7A-low groups based on the normalized single-cell expression levels of ZBTB7A, with cells above the median expression value classified as ZBTB7A-high and those below as ZBTB7A-low. Pathway enrichment analysis at the single-cell level was performed using the GSVA R package (version 1.46.0; https://bioconductor.org/packages/GSVA). Gene sets were obtained from MSigDB (https://www.gsea-msigdb.org/)., including the Hallmark Wnt/β-catenin and Hippo signaling pathways. Differential pathway activities between ZBTB7A-high and ZBTB7A-low tumor cells were subsequently compared.

Cell lines and culture conditions. The human ovarian epithelial cell line IOSE80 was obtained from The Cell Bank of Type Culture Collection of The Chinese Academy of Sciences, and the OV cell lines (SKOV3, OVCAR3, A2780 and CAOV3) were obtained from American Type Culture Collection. 293T cells were also obtained from American Type Culture Collection. IOSE80, SKOV3 and OVCAR3 cells were maintained in RPMI-1640 (cat. no. 11875-093; Gibco, Thermo Fisher Scientific, Inc.) supplemented with 10% FBS (cat. no. 10099-141; Gibco, Thermo Fisher Scientific, Inc.) and 1% penicillin/streptomycin (cat. no. 15140-122; Gibco, Thermo Fisher Scientific, Inc.). A2780 cells were maintained in RPMI-1640 supplemented with 10% FBS and 2 mM L-glutamine (cat. no. 25030-081; Gibco, Thermo Fisher Scientific, Inc.). CAOV3 and 293T cells were cultured in Dulbecco's Modified Eagle Medium (cat. no. 11965-092; Gibco, Thermo Fisher Scientific, Inc.) supplemented with 10% FBS. All cells were incubated at 37˚C in a humidified atmosphere containing 5% CO_2.

Plasmid construction. For ZBTB7A overexpression (ZBTB7A-OE), the full-length human ZBTB7A coding sequence (CDS) was amplified by PCR from a cDNA library generated in our laboratory from 293T cells. Briefly, 293T cell RNA was extracted using TRIzol reagent (cat. no. 15596026; Invitrogen; Thermo Fisher Scientific, Inc.) and reverse-transcribed using the SuperScript™ IV First-Strand Synthesis System (cat. no. 18091050; Invitrogen; Thermo Fisher Scientific, Inc.), according to the manufacturer's instructions, to generate the cDNA library. PCR amplification was performed using Q5® High-Fidelity DNA Polymerase (cat. no. M0491; New England Biolabs, Inc.). The CDS was confirmed to match the reference sequence (NM_015898.4). Primers were designed to introduce *Hin*dIII and *Xho*I restriction sites for directional cloning. The primer sequences were as follows: Forward primer, 5'-CCC AAGCTTATGGACGACGACGACGACG-3'; reverse primer, 5'-CCGCTCGAGTCAGGCGGCTGCTGC TG-3'. PCR was carried out under the following thermocycling conditions: Initial denaturation at 98˚C for 30 sec; followed by 35 cycles of denaturation at 98˚C for 10 sec, annealing at 60˚C for 20 sec and extension at 72˚C for 90 sec; followed by a final extension at 72˚C for 2 min.

The PCR-amplified fragment was digested with *Hin*dIII and *Xho*I restriction enzymes (New England Biolabs, Inc.) and subcloned into the mammalian expression vector pcDNA3.1 (cat. no. V79520; Invitrogen; Thermo Fisher Scientific, Inc.). For transient transfection, OVCAR3 cells were seeded in 6-well plates at a density of $2.0x10^5$ cells/well and allowed to adhere overnight. The cells were transfected with ZBTB7A-OE plasmid or the corresponding empty pcDNA3.1 vector (negative control) using Lipofectamine® 3000 transfection reagent (Invitrogen, Thermo Fisher Scientific) according to the manufacturer's protocol. Briefly, 2.5 μg plasmid DNA was used per well and transfection was performed at 37˚C for 6 h, after which the medium was replaced with fresh complete medium. Cells were collected or subjected to subsequent experiments 24-48 h post-transfection (24 h for RT-qPCR; 48 h for western blotting), unless otherwise specified.

In addition, the CRLF1 promoter region, encompassing -900 to +100 bp relative to the transcription start site (TSS), was amplified by PCR using genomic DNA extracted from 293T cells as the template. Genomic DNA was isolated using a commercial genomic DNA extraction kit (TIANamp Genomic DNA Kit; Tiangen Biotech Co., Ltd.), according to the manufacturer's instructions. PCR amplification was performed using a high-fidelity DNA polymerase (Q5 High-Fidelity DNA Polymerase). Primers were designed to introduce *Kpn*I and *Xho*I restriction sites at the 5'-ends for directional cloning. The primer sequences were as follows: Forward, 5'- GCG CGGGGTACCTTTTTCCGTGGCGGGGTGTGAATA G-3'; reverse, 5'-CCGCGCCTCGAGGGCGGTGGCGCAGGG CGCGG-3'. PCR was carried out under the following thermocycling conditions: Initial denaturation at 98˚C for 30 sec; followed by 35 cycles of denaturation at 98˚C for 10 sec, annealing at 72˚C for 20 sec and extension at 72˚C for 30 sec; followed by a final extension at 72˚C for 2 min. The PCR product was digested with *Kpn*I and *Xho*I restriction enzymes (New England Biolabs, Inc.), and was subsequently subcloned into the pGL3-Basic luciferase reporter vector (Promega Corporation). This reporter construct was used for luciferase assays.).

Small interfering RNA (siRNA) knockdown. For knockdown, RNA interference experiments were performed using chemically synthesized siRNAs. Validated siRNAs targeting ZBTB7A (si-ZBTB7A) and CRLF1 (si-CRLF1), as well as a scrambled negative control (NC) siRNA (si-NC), were purchased from Shanghai GenePharma Co., Ltd. The sequences were as follows: si-ZBTB7A, sense 5'-GGCGAC GUGGUGAUCCUGG dTdT-3', antisense 5'-CCAGGAUCA CCACGUCGCC dTdT-3'; si-CRLF1, sense 5'-CACGCU GGAUAUCCUGGAU dTdT-3', antisense 5'-GUGCGACCU AUAGGACCUA dTdT-3'; and si-NC, sense 5'-UUCUCC

GAACGUGUCACGU dTdT-3' and antisense 5'-ACGUGA CACGUUCGGAGAA dTdT-3'. For siRNA transfection, A2780 cells were seeded in 6-well plates at a density of $2.0x10^5$ cells/well and allowed to adhere overnight. The cells were then transfected with si-ZBTB7A, si-CRLF1 or si-NC using Lipofectamine 3000 according to the manufacturer's protocol. Briefly, siRNAs were used at a final concentration of 50 nM/well and transfection was performed at 37˚C for 6 h, after which the medium was replaced with fresh complete medium. Knockdown efficiency was evaluated 24 h after transfection by RT-quantitative PCR (RT-qPCR) and western blotting.

RNA extraction and RT-qPCR. Total RNA was extracted from IOSE80, SKOV3, OVCAR3, A2780 and CAOV3 cells by using TRIzol Reagent according to the manufacturer's protocol. RNA concentration and purity were assessed using a NanoDrop One Spectrophotometer (NanoDrop; Thermo Fisher Scientific, Inc.), and only samples with A260/A280 ratios between 1.8 and 2.0 were used for subsequent experiments. RT was performed using the PrimeScript™ RT Reagent Kit with gDNA Eraser (cat. no. RR047A; Takara Bio, Inc.) according to the manufacturer's instructions. Briefly, 1 μg total RNA was treated with gDNA Eraser to remove genomic DNA contamination, followed by first-strand cDNA synthesis in a total reaction volume of 20 μl. qPCR was performed using PowerUp™ SYBR™ Green Master Mix (cat. no. A25742; Applied Biosystems, Thermo Fisher Scientific) on ABI 7500 Fast Real-Time PCR System (Applied Biosystems; Thermo Fisher Scientific, Inc.). The thermocycling conditions were as follows: Initial UDG activation at 50˚C for 2 min and initial denaturation at 95˚C for 2 min, followed by 40 cycles of denaturation at 95˚C for 15 sec and annealing/extension at 60˚C for 1 min. A melting curve analysis was conducted post-amplification to verify the specificity of the PCR products. All reactions were performed in triplicate. Expression levels were normalized to GAPDH as the endogenous control. The relative quantification of gene expression was calculated using the $2^{-\Delta\Delta Cq}$ method (28). The following primers were used and synthesized by Sangon Biotech Co., Ltd.: ZBTB7A, forward 5'-GCAACATCTGCAAGGTCCGCTT-3', reverse 5'-TCT TCAGGTCGTAGTTGTGGGC-3'; CRLF1, forward 5'-GAG ACCTTCCTCCACACCAACT-3', reverse 5'-CATAGGGCG TAAAGAGAGCCAG-3'; and GAPDH, forward 5'-GTCTCC TCTGACTTCAACAGCG-3', reverse ACCACCCTGTTG CTGTAGCCAA-3'.

Western blotting. Total protein was extracted from IOSE80, SKOV3, OVCAR3, A2780 and CAOV3 cell using RIPA lysis buffer (cat. no. P0013B; Beyotime Biotechnology) supplemented with protease and phosphatase inhibitors (cat. nos. 04693159001 and 04906837001; Roche Diagnostics). Lysates were incubated on ice for 30 min with vortexing every 10 min, then centrifuged at 12,000 x g for 15 min at 4˚C to collect the supernatant. Western blotting was performed as described in our previous study (29). Briefly, protein concentrations were determined using a BCA Protein Assay Kit (cat. no. 23225; Thermo Fisher Scientific, Inc.) following the manufacturer's instructions. Subsequently, proteins (~20 μg) were separated by SDS-PAGE on 8% gels and transferred onto PVDF membranes, which were blocked in 5% non-fat milk in Tris-buffered saline with 0.1% Tween-20 (TBST) for 1 h at room temperature. The membranes were then incubated overnight at 4˚C with the following primary antibodies: Anti-ZBTB7A (rabbit polyclonal; cat. no. ab70208; 1:1,000; Abcam), anti-CRLF1 (rabbit polyclonal; cat. no. ab211438; 1:1,000; Abcam), phosphorylated (p)-AKT (rabbit monoclonal; cat. no. 4060; 1:1,000; Cell Signaling Technology, Inc.), AKT (rabbit monoclonal; cat. no. 4691; 1:1,000; Cell Signaling Technology, Inc.) and anti-GAPDH (mouse monoclonal; cat. no. ab8245; 1:5,000; Abcam). After three 10-min washes in TBST, the membranes were incubated for 1 h at room temperature with HRP-conjugated goat anti-rabbit IgG (cat. no. 7074; 1:5,000) or goat anti-mouse IgG (cat. no. 91196; 1:5,000) secondary antibodies (both from Cell Signaling Technology, Inc.). Protein bands were visualized using ECL reagent (cat. no. 32106; Thermo Fisher Scientific, Inc.) and images were captured using the ChemiDoc XRS+ imaging system (Bio-Rad Laboratories, Inc.). Band intensities were semi-quantified using ImageJ software (version 1.53c; National Institutes of Health), and GAPDH was used as an internal loading control.

Prediction of ZBTB7A downstream target genes. Target genes were predicted using three complementary TF-target prediction resources: hTFtarget (https://guolab.wchscu.cn/hTFtarget/#!/), GRID (https://www.grid.ac/), and ChIP-Atlas (https://chip-atlas.org). For hTFtarget and GRID, predicted targets of ZBTB7A were retrieved based on curated TF-target regulatory relationships. For ChIP-Atlas, ZBTB7A ChIP-seq datasets were queried using the 'Target Genes' function with default parameters. Candidate genes consistently identified across all three databases were considered high-confidence ZBTB7A downstream targets. The position weight matrix of ZBTB7A was retrieved from the JASPAR database (https://jaspar.genereg.net), and promoter annotations were obtained from the Eukaryotic Promoter Database (EPD; https://epd.epfl.ch).

Cell Counting Kit-8 (CCK-8). Cell viability was assessed using CCK-8 (cat. no. CK04-11; Dojindo Laboratories, Inc.) according to the manufacturer's instructions. Briefly, OV cells (OVCAR3 or A2780) were seeded into 96-well plates at a density of $2x10^3$ cells/well in 100 μl complete medium and allowed to adhere overnight. At the indicated time points (0, 24, 48 and 72 h), 10 μl CCK-8 solution was added to each well and incubated for 2 h at 37˚C in a humidified incubator containing 5% CO_2. Absorbance was measured at 450 nm using a microplate reader (BioTek Synergy H1; Agilent Technologies, Inc.). Each condition was tested in triplicate and experiments were repeated independently at least three times.

EdU assay. Cell proliferation was assessed using the Click-iT™ EdU Alexa Fluor™ 488 Imaging Kit (cat. no. C10337; Invitrogen; Thermo Fisher Scientific, Inc.) according to the manufacturer's protocol. Briefly, A2780 and OVCAR3 cells were seeded into 24-well plates containing sterile glass coverslips at a density of $5x10^4$ cells/well and cultured overnight. The following day, the cells were incubated with 10 μM EdU working solution for 2 h at 37˚C under 5% CO_2. Subsequently,

the cells were fixed with 4% paraformaldehyde for 15 min at room temperature and permeabilized with 0.5% Triton X-100 in PBS for 20 min. The Click-iT reaction cocktail containing Alexa Fluor 488 azide was then added and allowed to react in the dark for 30 min at room temperature. After washing, the nuclei were counterstained with DAPI (5 μg/ml) for 10 min at room temperature. Coverslips were mounted onto glass slides using anti-fade mounting medium and images were captured using a fluorescence microscope (Leica DMi8 or equivalent; Leica Microsystems, Inc.).

Colony formation assay. Clonogenic potential was evaluated using a standard crystal violet staining assay. Briefly, A2780 and OVCAR3 cells were seeded into 6-well plates at a low density of 500 cells/well, and incubated for 10-14 days under standard culture conditions (37˚C, 5% CO_2). During this period, the culture medium was replaced every 3-4 days to ensure optimal growth. Once visible colonies (≥50 cells/colony) had formed, the plates were gently washed twice with PBS and colonies were fixed with 4% paraformaldehyde for 15 min at room temperature. After fixation, the cells were stained with 0.1% crystal violet solution (prepared in 20% methanol; MilliporeSigma) for 20-30 min at room temperature, followed by thorough rinsing with distilled water to remove excess stain. Finally, the plates were air-dried and images were captured.

Transwell migration assays. Cell migration ability was evaluated using 24-well Transwell chambers with 8.0-μm pore polycarbonate membranes (cat. no. 3422; Costar, Corning, Inc.). Briefly, the cells were serum-starved for 12 h prior to seeding. Subsequently, ~1x10^5 OVCAR3 cells suspended in 200 μl serum-free medium were added to the upper chamber of each insert, whereas 600 μl complete medium containing 10% FBS was placed in the lower chamber as a chemoattractant. After incubation for 24 h at 37˚C in a humidified incubator with 5% CO_2, non-migrating cells on the upper surface of the membrane were gently removed using a cotton swab. Migrated cells on the lower surface were fixed with 4% paraformaldehyde for 15 min at room temperature and then stained with 0.1% crystal violet for 20 min. The membranes were rinsed gently with PBS and allowed to air dry. Images of stained cells in at least five randomly selected fields per insert were captured under a light microscope (x200 magnification; Olympus Corporation).

Chromatin immunoprecipitation (ChIP)-qPCR. ChIP was performed as previously described with minor modifications (30). Briefly, OVCAR3 cells were crosslinked with 1% formaldehyde at room temperature for 10 min and quenched with 125 mM glycine for 5 min at room temperature. The cells were then washed with cold PBS, lysed with ChIP lysis buffer provided in the Magna ChIP™ A/G Chromatin Immunoprecipitation Kit (cat. no. 17-10085; MilliporeSigma) and chromatin was sheared by sonication on ice using a Bioruptor sonicator (Diagenode SA) with 30 sec on/30 sec off cycles for a total of 10-15 min (fixed-frequency sonication; instrument settings: High power), to generate an average DNA fragment size of 200-500 bp. Equal amounts of chromatin (corresponding to 20 μg DNA per immunoprecipitation) were incubated overnight at 4˚C with anti-ZBTB7A (2 μg per reaction; cat. no. ab70208; Abcam) or normal rabbit IgG as a negative control (2 μg per reaction; cat. no. ab171870; Abcam). Immunocomplexes were captured using 25 μl Protein A/G magnetic beads (cat. no. 88802; Thermo Fisher Scientific, Inc.) for 2 h at 4˚C with rotation. The beads were sequentially washed with low-salt buffer (20 mM Tris-HCl (pH 8.1), 150 mM NaCl, 2 mM EDTA, 1% Triton X-100, 0.1% SDS), high-salt buffer (same as low-salt but with 500 mM NaCl), LiCl buffer (10 mM Tris-HCl (pH 8.1), 250 mM LiCl, 1 mM EDTA, 1% NP-40, 1% sodium deoxycholate) and TE buffer (10 mM Tris-HCl (pH 8.0), 1 mM EDTA). Crosslinks were reversed at 65˚C overnight, and the samples were then treated with RNase A (0.2 mg/ml) at 37˚C for 30 min, followed by proteinase K (0.2 mg/ml) at 55˚C for 2 h. Subsequently, DNA was purified and subjected to qPCR using SYBR Green Master Mix (cat. no. A25742; Applied Biosystems; Thermo Fisher Scientific, Inc.) on an ABI 7500 Fast Real-Time PCR System (Applied Biosystems; Thermo Fisher Scientific, Inc.), under the following thermocycling conditions: Initial denaturation at 95˚C for 2 min, followed by 40 cycles at 95˚C for 15 sec and 60˚C for 30 sec. Primer sequences used for ChIP-qPCR were as follows: CRLF1 promoter (ZBTB7A-binding region), forward 5'-ATCTCTGTGTACAAGGGTGCT-3', reverse 5'-TTTCTAGGGAGGGTGGGAGTC-3'. ChIP enrichment was calculated as percentage of input (%Input) using the formula: $\%Input=100x2^{(Cq\_Input-Cq\_IP)}$ x dilution factor.

Luciferase reporter assay. To assess the transcriptional regulation of CRLF1 by ZBTB7A, a dual-luciferase reporter assay was conducted using the Dual-Luciferase® Reporter Assay System (cat. no. E1910; Promega Corporation). The 1 kb promoter region of CRLF1 (-900 to +100 bp relative to the TSS) was cloned into the pGL3-Basic vector (Promega Corporation) using *Kpn*I and *Xho*I restriction sites to generate the firefly luciferase reporter plasmid (CRLF1-Luc). Full-length human ZBTB7A cDNA was cloned into the pcDNA3.1(+) expression vector to generate the ZBTB7A-OE construct. Subsequently, 293T cells were seeded in 24-well plates at a density of 1.5x10^5 cells/well and cultured overnight. The cells were then co-transfected with 400 ng pGL3-CRLF1-Luc reporter construct, 100 ng pRL-TK *Renilla* luciferase control vector (cat. no. E2241; Promega Corporation) and 500 ng either ZBTB7A-pcDNA3.1 or empty pcDNA3.1 vector (as a control) using Lipofectamine 3000 transfection reagent, according to the manufacturer's instructions. After 48 h of incubation, the cells were harvested and luciferase activity was measured using the Dual-Luciferase Reporter Assay System on a luminometer (GloMax 20/20; Promega Corporation). Firefly luciferase activity was normalized to *Renilla* luciferase activity to control for transfection efficiency. All experiments were performed in triplicate and repeated at least three times independently.

Statistical analysis. All statistical analyses were performed using GraphPad Prism 9.0 (Dotmatics). Quantitative data are presented as the mean ± SD from at least three independent experiments. Two-group comparisons were evaluated using the unpaired two-tailed Student's t-test. Comparisons among multiple groups were performed using one-way analysis of variance followed by Tukey's post hoc test. $P<0.05$ was

Table I. Univariate and multivariate Cox regression analyses for overall survival in The Cancer Genome Atlas-ovarian cancer cohort.

Variable	Model	HR	95% CI	P-value
ZBTB7A (high vs. low)	Univariate	1.38	1.01-1.88	0.042
ZBTB7A (high vs. low)	Multivariate (adjusted for age and grade)	1.43	1.05-1.96	0.024
CRLF1 (high vs. low)	Univariate	1.33	0.98-1.81	0.070
CRLF1 (high vs. low)	Multivariate (adjusted for age and grade)	1.39	1.02-1.90	0.036
Age (per 1-year)	Multivariate (including ZBTB7A, age and grade)	1.02	1.01-1.04	0.003
Age (per 1-year)	Multivariate (including CRLF1, age and grade)	1.02	1.01-1.04	0.0048

CI, confidence interval; CRLF1, cytokine receptor-like factor 1; HR, hazard ratio; ZBTB7A, zinc finger and BTB domain-containing 7A.

considered to indicate a statistically significant difference. All experiments were independently repeated at least three times to ensure reproducibility.

Results

ZBTB7A is upregulated in OV and is associated with adverse OS. To identify DEGs in OV, four independent OV GEO datasets (GSE26712, GSE160626, GSE143897 and GSE119168) were analyzed. Each dataset revealed widespread transcriptional changes between tumor and normal tissues (Fig. 1A-D). By intersecting the results, 168 common dysregulated genes across all four cohorts were obtained. Among these, ZBTB7A appeared consistently upregulated and was highlighted in a representative volcano plot (Fig. 1F). To further evaluate the clinical relevance of ZBTB7A, its expression was examined in pan-cancer datasets. As shown in Fig. 1G, ZBTB7A was broadly elevated across multiple tumor types, with OV showing one of the most significant increases. A direct comparison of tumor and healthy ovarian samples (TNMplot) confirmed this result, showing a significant increase in ZBTB7A expression in ovarian tumor samples (Fig. 1H). Protein-level evidence was obtained from the Human Protein Atlas (HPA) dataset, where immunohistochemistry images indicated stronger nuclear staining of ZBTB7A in OV samples relative to healthy ovarian tissues (Fig. 1I). Consistently, Kaplan-Meier survival analysis revealed that higher ZBTB7A expression was significantly associated with a shorter OS (log-rank P=0.038; Fig. 1J). Overall, these results demonstrated that ZBTB7A was significantly upregulated in OV and could serve as a marker of poor prognosis. Univariate and multivariate Cox regression analyses using TCGA-OV cohort further identified ZBTB7A expression as an independent prognostic factor for OS after adjustment for age and tumor grade (Table I).

Single-cell analysis localizes ZBTB7A to tumor cells and links it to aggressive programs. To further characterize the cellular distribution and functional associations of ZBTB7A in OV, a single-cell RNA-seq dataset of ovarian tumors was analyzed. UMAP clustering identified the major cell populations, including malignant epithelial cells, fibroblasts, endothelial cells, monocytes, T cells and B cells, each defined by canonical marker expression (Fig. 2A and B). Module scoring confirmed that the annotated clusters captured expected lineage-specific signatures (Fig. 2C-H). Next, downstream analyses were restricted to the malignant epithelial (tumor) compartment, and tumor cells were stratified into ZBTB7A-high and ZBTB7A-low groups (Fig. 2I). Notably, tumor cells exhibiting high ZBTB7A expression displayed markedly increased scores for migration, EMT and proliferation compared with ZBTB7A-low counterparts (Fig. 2J-L). Pathway enrichment at the single-cell level further supported these associations. ZBTB7A-high tumor cells showed higher activities of the Wnt/β-catenin and Hippo-YAP signaling pathways, both of which are well known to drive OV progression (Fig. 2M and N). Together, these analyses demonstrate that within the tumor cell compartment, high ZBTB7A may mark an aggressive transcriptional state characterized by enhanced motility, EMT, proliferative drive and activation of malignancy-associated pathways.

ZBTB7A promotes the proliferation and migration of OV cells. To determine the functional role of ZBTB7A in OV cells, the endogenous expression of ZBTB7A across a panel of human ovarian cell lines was first examined, including the normal ovarian surface epithelial line IOSE80, and the OV cell lines SKOV3, OVCAR3, A2780 and CAOV3. RT-qPCR and western blotting revealed that ZBTB7A was expressed at varying levels across these cells, with relatively high expression in A2780 and the lowest expression observed in OVCAR3 cells among the OV cell lines (Fig. 3A and B). Subsequently, OVCAR3 cells, which showed the lowest basal ZBTB7A expression, were selected for overexpression experiments, and successful overexpression was confirmed at both the mRNA and protein levels (Fig. 3C and D).

Functionally, overexpression of ZBTB7A in OVCAR3 cells markedly promoted malignant phenotypes. In the CCK-8 assay, ZBTB7A-OE cells displayed a clear, time-dependent increase in viability compared with that in the vector control group (Fig. 3E). The EdU incorporation assay further confirmed this proliferative advantage, as ZBTB7A-OE cells exhibited a higher proportion of EdU-positive nuclei, reflecting enhanced DNA synthesis and cell-cycle progression (Fig. 3F). To extend these findings, a colony formation assay was performed, which demonstrated that ZBTB7A significantly increased clonogenic potential, with overexpressing cells forming a greater number of larger colonies compared with that in the control group. In addition, the Transwell assay showed a significant increase

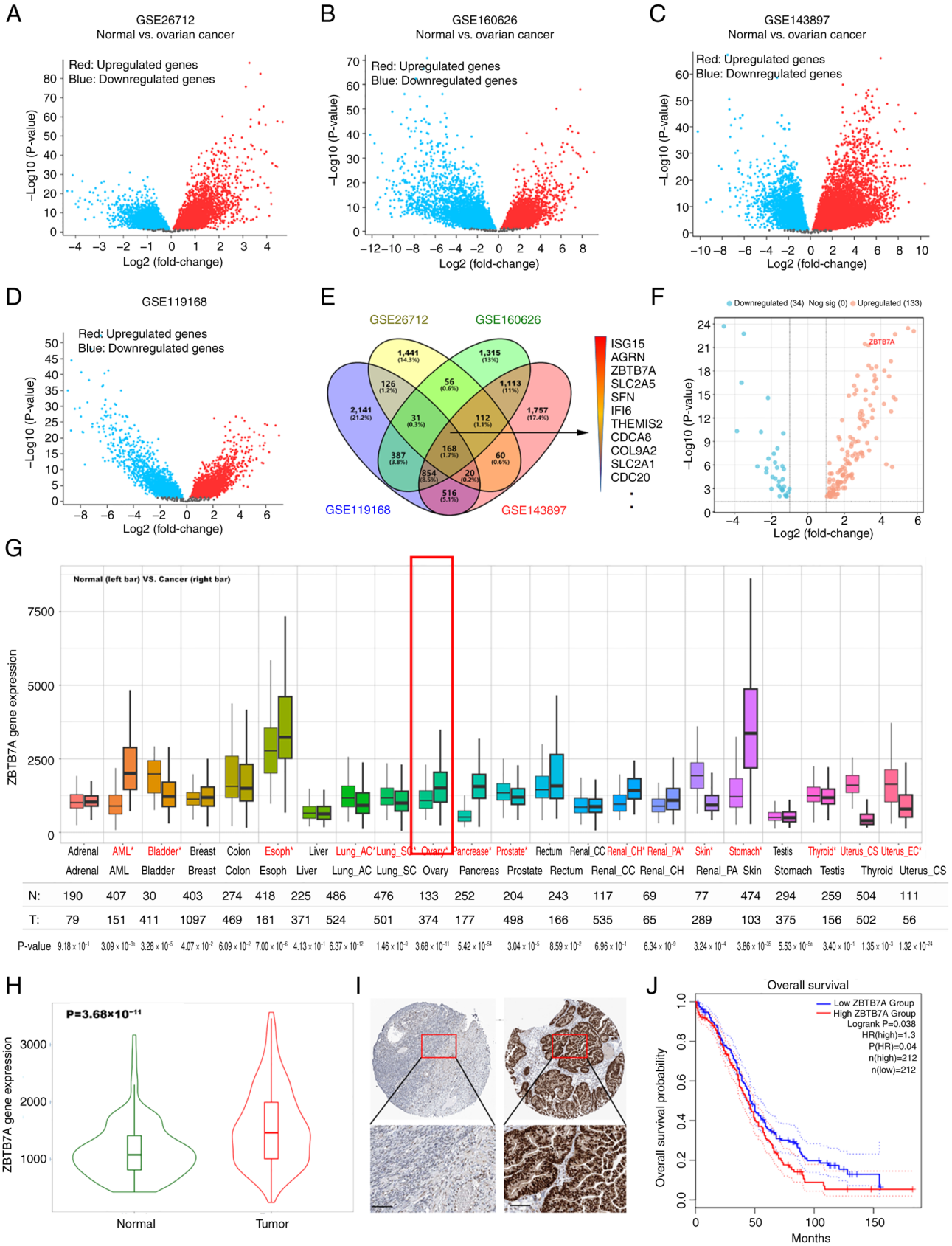

Figure 1. ZBTB7A is upregulated in ovarian cancer and is associated with a poor prognosis. Volcano plots showing differentially expressed genes in ovarian cancer vs. normal tissue in (A) GSE26712, (B) GSE160626, (C) GSE143897 and (D) GSE119168 datasets. (E) Venn diagram of common dysregulated genes across all four datasets. (F) ZBTB7A highlighted in a representative volcano plot. (G) Pan-cancer analysis of ZBTB7A expression from the TNMplot database; the two boxplots for each tissue represent normal (left) and tumor samples (right). Cancer types labeled in red indicate a significant difference (P<0.05). Ovarian cancer is marked in a red box. *P<0.05. (H) ZBTB7A was significantly upregulated in ovarian cancer compared with in normal tissues (TNMplot). (I) Immunohistochemical staining of ZBTB7A in normal and tumor tissues (Human Protein Atlas database). Scale bar, 100 μm. (J) Kaplan-Meier survival curve showing that high ZBTB7A expression was associated with worse overall survival (Gene Expression Profiling Interactive Analysis). ZBTB7A, zinc finger and BTB domain-containing 7A.

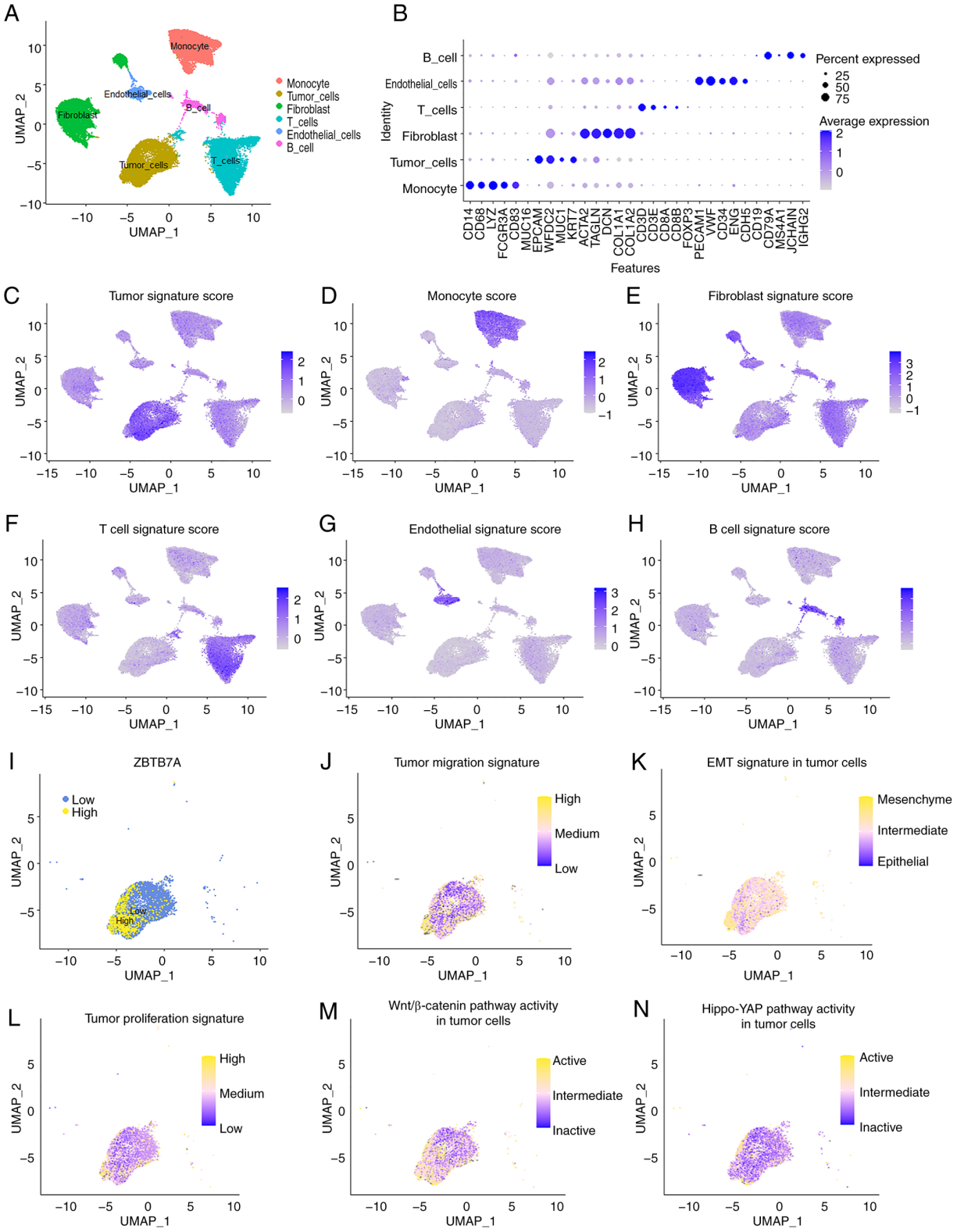

Figure 2. Single-cell analysis reveals that ZBTB7A expression localizes to malignant epithelial cells and is associated with aggressive phenotypes. This figure was generated using Seurat. (A) UMAP plot showing cell type clustering. (B) Marker gene expression of different cell clusters. (C) Tumor signature score for lineage markers. (D) Monocyte score for lineage markers. (E) Fibroblast signature score for lineage markers. (F) T cell signature score for lineage markers. (G) Endothelial signature score for lineage markers. (H) B cell score for lineage markers. (I) Stratification of tumor cells into ZBTB7A-high and ZBTB7A-low subsets. Enrichment of (J) migration, (K) EMT and (L) proliferation programs in ZBTB7A-high tumor cells. Pathway scores show increased (M) Wnt/β-catenin and (N) Hippo-YAP signaling in ZBTB7A-high cells. EMT, epithelial-mesenchymal transition; UMAP, Uniform Manifold Approximation and Projection; ZBTB7A, zinc finger and BTB domain-containing 7A.

in the number of migrating cells in the ZBTB7A-OE group, indicating that ZBTB7A may promote a more migratory phenotype (Fig. 3H). Taken together, these gain-of-function experiments indicated that ZBTB7A-OE could enhance cell

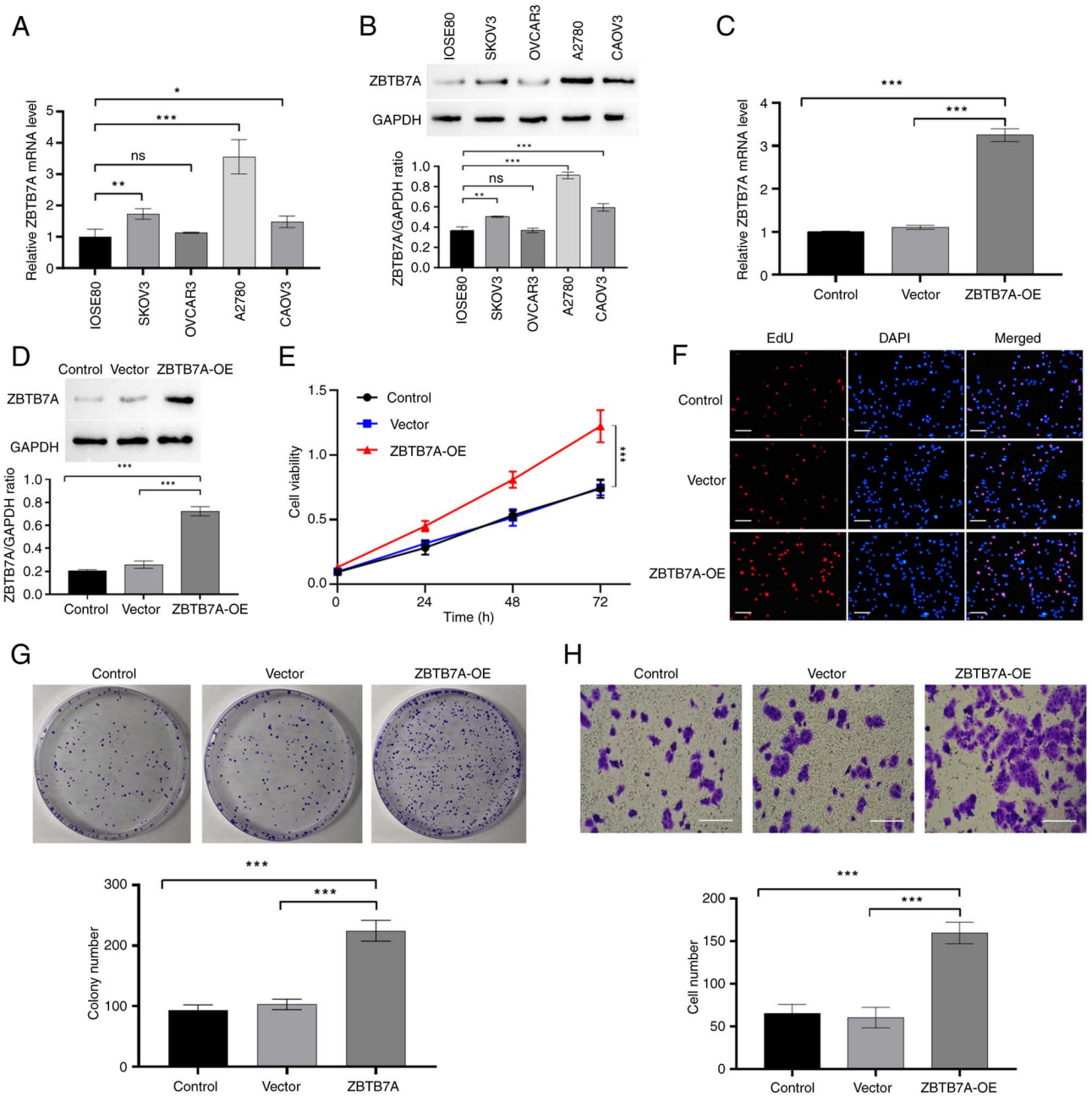

Figure 3. ZBTB7A-OE promotes the proliferation and migration of ovarian cancer cells. Endogenous ZBTB7A (A) mRNA and (B) protein expression across different ovarian cancer cell lines. ZBTB7A-OE efficacy in OVCAR3 cells was analyzed by (C) reverse transcription-quantitative PCR and (D) western blotting. (E) Cell Counting Kit-8 assay showing increased viability. (F) EdU incorporation assay indicating enhanced proliferation. Scale bar, 100 μm. (G) Colony formation assay showing increased clonogenicity. (H) Transwell assay showing enhanced migration. Scale bar, 50 μm. *P<0.05, **P<0.01, ***P<0.001. ns, not significant; OE, overexpression; ZBTB7A, zinc finger and BTB domain-containing 7A.

viability, proliferation, clonogenic survival and motility, supporting a pro-oncogenic role for ZBTB7A in OV.

ZBTB7A knockdown suppresses the proliferation and migration of OV cells. To complement the overexpression studies, the present study investigated the effects of ZBTB7A loss-of-function. Basal expression profiling indicated that A2780 cells expressed relatively high levels of ZBTB7A, and were therefore selected for knockdown experiments. Transfection with si-ZBTB7A effectively reduced both the mRNA and protein levels of ZBTB7A, as confirmed by RT-qPCR and western blotting (Fig. 4A and B).

Functionally, silencing ZBTB7A significantly impaired OV cell behaviors. In the CCK-8 assays, si-ZBTB7A A2780 cells exhibited markedly reduced viability compared with that in the si-NC cells (Fig. 4C). The EdU assay further confirmed diminished proliferative activity, with a lower proportion of EdU-positive nuclei following ZBTB7A knockdown (Fig. 4D). Moreover, long-term colony formation assays revealed a significant reduction in both the number and size of colonies, indicating a loss of clonogenic potential in si-ZBTB7A A2780 cells (Fig. 4E). Similarly, the Transwell assay showed that ZBTB7A knockdown markedly decreased the number of migrating A2780 cells, reflecting impaired motility (Fig. 4F).

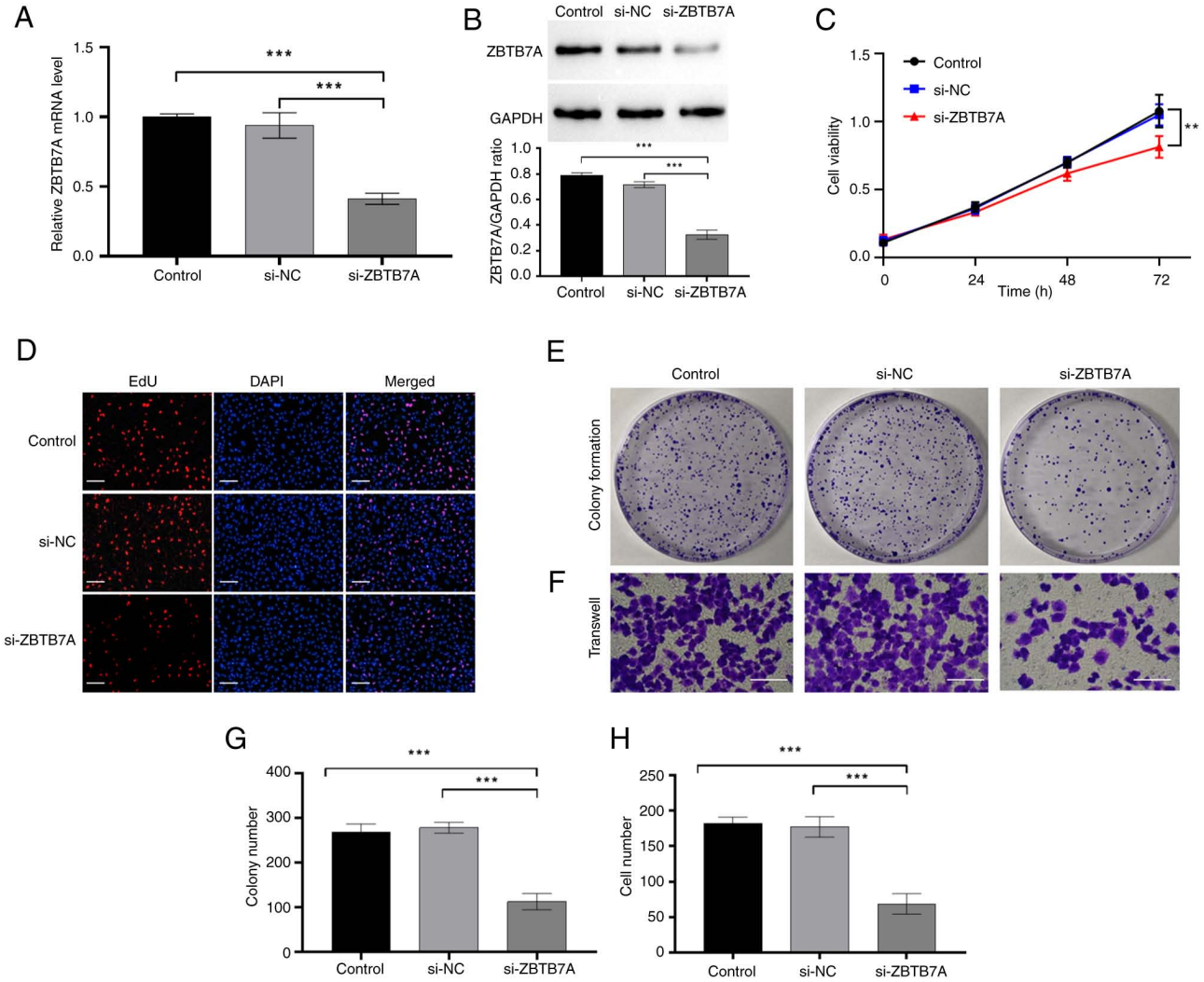

Figure 4. ZBTB7A knockdown inhibits the proliferation and migration of ovarian cancer cells. ZBTB7A knockdown efficacy was analyzed by (A) reverse transcription-quantitative PCR and (B) western blotting (C) Cell Counting Kit-8 assay showing increased viability. (D) EdU assay confirming reduced proliferation. Scale bar, 100 μm. (E and G) Representative images of colony formation assays in the indicated groups and semi-quantification of colony numbers from three independent experiments. Scale bar, 50 μm. (F and H) Representative images of Transwell assay and semi-quantification of Transwell cell numbers from three independent experiments. **P<0.01, ***P<0.001. NC, negative control; si, small interfering; ZBTB7A, zinc finger and BTB domain-containing 7A.

Semi-quantitative analyses consistently supported these inhibitory effects (Fig. 4G and H). Together, these results provided strong evidence that ZBTB7A was required for promoting the proliferation, clonogenic survival and migration of OV cells, reinforcing its role as an oncogenic driver.

CRLF1 is identified as a downstream target of ZBTB7A and is clinically relevant in OV. Given that ZBTB7A is a classical TF, the present study aimed to predict its potential downstream targets. To identify these targets, the findings of three complementary TF-target prediction platforms were combined: hfTarget, GRID and ChIP-Atlas. Cross-database intersection analysis revealed three overlapping candidate genes: CDC27, CRLF1 and LUC7L, which were consistently predicted to be regulated by ZBTB7A. Subsequently, the correlation between these candidates and ZBTB7A was analyzed in TCGA-OV cohort. The results revealed that CDC27 expression exhibited a moderate positive correlation with ZBTB7A, whereas CRLF1 and LUC7L showed weak but significant correlations with ZBTB7A, suggesting that they may indeed be co-regulated (Fig. 5B). The prognostic value of these candidates was then assessed. Kaplan-Meier analysis revealed that higher expression of CRLF1, but not CDC27 or LUC7L, was significantly associated with a poorer OS in patients with OV (Fig. 5C). Notably, survival analysis revealed that only CRLF1 mirrored the clinical outcome pattern of ZBTB7A. Based on this concordance between expression, correlation and prognostic outcome, CRLF1 was selected as the most relevant downstream candidate for further analysis. Next, CRLF1 expression was also analyzed in pan-cancer datasets. As shown in Fig. 5D, CRLF1 was elevated in several tumor types, with OV displaying one of the most significant increases. Consistent with this, direct comparison between ovarian tumor and healthy samples confirmed significantly increased CRLF1 expression (Fig. 5E).

In univariate Cox regression, high ZBTB7A expression was associated with an increased risk of death (HR=1.38, 95% CI: 1.01-1.88, P=0.042), and high CRLF1 expression showed a similar trend, but this was not significant (HR=1.33, 95% CI: 0.98-1.81) (Table I). To determine whether ZBTB7A

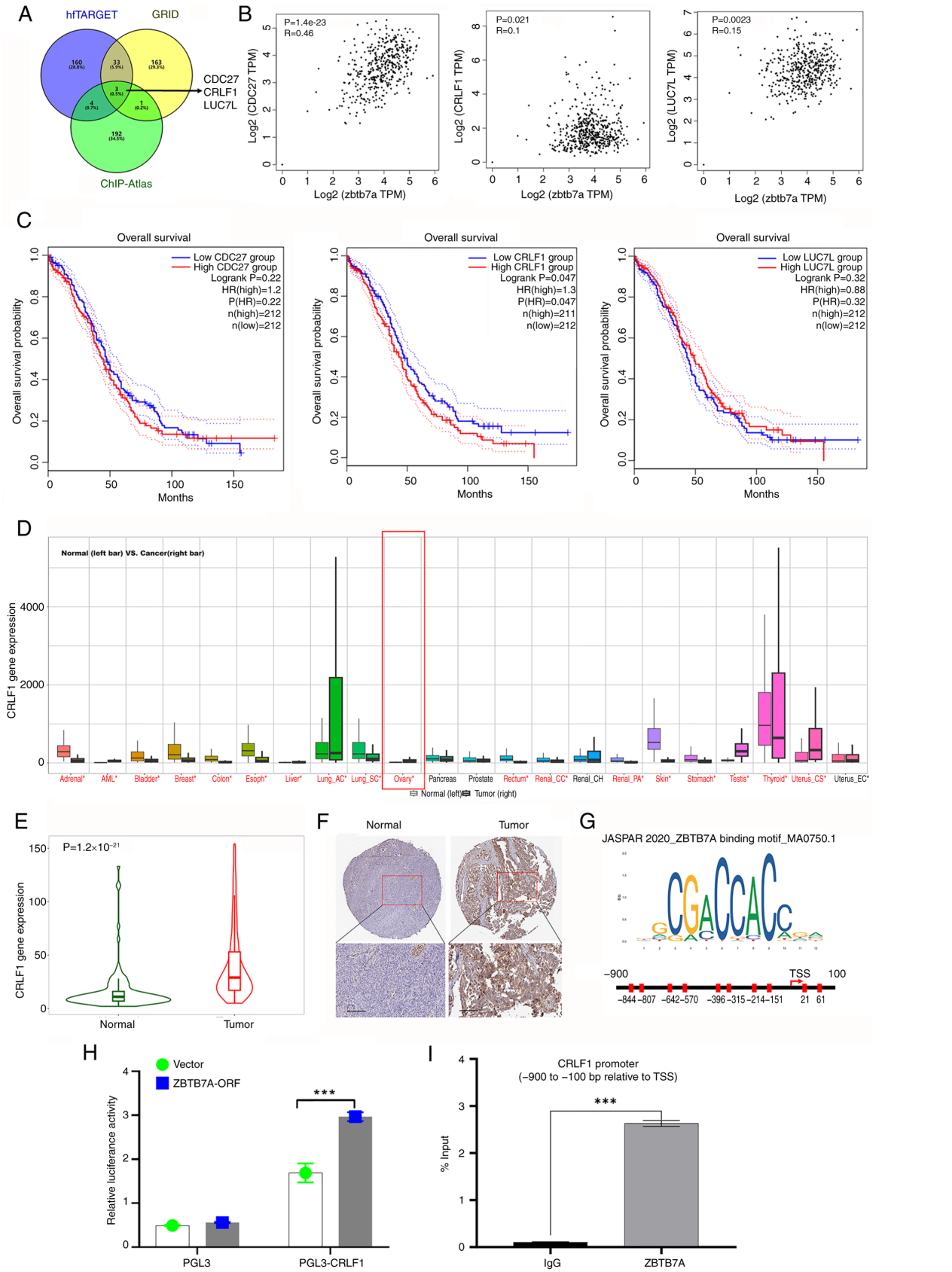

Figure 5. ZBTB7A transcriptionally regulates CRLF1 in ovarian cancer. (A) Venn diagram of predicted ZBTB7A targets. (B) Correlation analysis of ZBTB7A with CDC27, CRLF1 and LUC7L. (C) Kaplan-Meier survival analysis for each candidate (Gene Expression Profiling Interactive Analysis). (D) CRLF1 expression is elevated in ovarian cancer (pan-cancer); the two boxplots for each tissue represent normal (left) and tumor samples (right). Cancer types labeled in red indicate a significant difference (P<0.05). Ovarian cancer is marked in a red box. *P<0.05. (E) CRLF1 expression is elevated in ovarian cancer (TNMplot). (F) Immunohistochemical analysis from the Human Protein Atlas confirmed upregulation of CRLF1. Scale bar, 100 μm. (G) ZBTB7A binding motifs and predicted promoter region. (H) Luciferase reporter assay validating CRLF1 transcriptional activation. (I) ChIP-quantitative PCR analysis assays were performed in OVCAR3 cells using an anti-ZBTB7A antibody or IgG control. ***P<0.001. ChIP, chromatin immunoprecipitation; CRLF1, cytokine receptor-like factor 1; ORF, open reading frame; TSS, transcription start site; ZBTB7A, zinc finger and BTB domain-containing 7A.

and CRLF1 are independent prognostic factors, multivariate Cox models adjusting for age and tumor grade were further constructed. High ZBTB7A expression remained significantly associated with poor OS (HR=1.43, 95% CI: 1.05-1.96, P=0.024), as did high CRLF1 expression (HR=1.39, 95% CI: 1.02-1.90, P=0.036). Age was also independently associated with OS (HR per 1-year increase=1.02, P<0.005), whereas tumor grade did not reach statistical significance in this cohort. These data indicated that both ZBTB7A and CRLF1 serve as independent adverse prognostic biomarkers in OV (Table I).

In addition, protein-level evidence from the HPA database further supported these findings: Immunohistochemistry revealed stronger CRLF1 staining in ovarian tumor tissues compared with in normal ovarian tissues (Fig. 5F). To further investigate the transcriptional regulation of CRLF1 by ZBTB7A, the binding motif of ZBTB7A was obtained from the JASPAR database, and the CRLF1 promoter region (-900 to +100 bp relative to the TSS) was defined based on the EPD. Potential ZBTB7A-binding sites within this promoter region were subsequently identified through motif scanning analysis (Fig. 5G). Subsequently, the 1 kb region of the CRLF1 promoter was cloned into the pGL3 vector to perform a luciferase assay, and the ZBTB7A open reading frame was cloned into the pcDNA3 vector for co-transfection into 293T cells. As shown in Fig. 5H, cells transfected with the CRLF1 promoter construct exhibited markedly higher luciferase activity compared with the empty vector control. Notably, ZBTB7A-OE further enhanced CRLF1 promoter activity, whereas no increase was observed in the pGL3 empty vector group (Fig. 5H). Moreover, ChIP-qPCR analysis demonstrated significant enrichment of ZBTB7A at the CRLF1 promoter region (-900 to -100 bp relative to the TSS), indicating that ZBTB7A may directly occupy the CRLF1 promoter in OVCAR3 cells (Fig. 5I). Together, these results demonstrated that ZBTB7A may directly enhance CRLF1 transcriptional activity through promoter binding, thereby establishing CRLF1 as a functional downstream effector that mediates the oncogenic role of ZBTB7A in OV.

CRLF1 mediates the oncogenic effects of ZBTB7A in OV cells. To assess whether CRLF1 acts downstream of ZBTB7A, its expression was examined following ZBTB7A-OE in OVCAR3 cells. Both RT-qPCR and western blotting confirmed that ZBTB7A-OE led to a significant increase in CRLF1 mRNA and protein levels (Fig 6A and B). Conversely, targeted knockdown of CRLF1 using a siRNA efficiently reduced its expression (Fig. S1), as verified by RT-qPCR and western blotting. Functional assays showed that knockdown of CRLF1 significantly attenuated the oncogenic phenotypes induced by ZBTB7A. Specifically, cells were co-transfected with the ZBTB7A-OE plasmid and siCRLF1, and the CCK-8 assay demonstrated that CRLF1 knockdown attenuated the enhanced cell viability induced by ZBTB7A-OE (Fig. 6C). Furthermore, the EdU assay confirmed that siCRLF1 blocked the ZBTB7A-OE-induced increase in DNA synthesis and proliferative activity (Fig. 6D). The colony formation assay further revealed that CRLF1 knockdown diminished both the number and size of colonies induced by ZBTB7A-OE (Fig. 6E). Finally, a Transwell migration assay showed that siCRLF1 markedly suppressed the pro-migratory effect of ZBTB7A-OE on OVCAR3 cells (Fig. 6F). Semi-quantitative analyses consistently demonstrated that CRLF1 knockdown largely reversed the proliferation and migration mediated by ZBTB7A (Fig. 6G and H). To further elucidate the downstream signaling mechanism, the activation status of the PI3K/AKT pathway was examined. Western blot analysis showed that ZBTB7A-OE significantly increased the levels of phosphorylated AKT, whereas CRLF1 knockdown markedly attenuated AKT phosphorylation without affecting total AKT expression (Fig. 6I). These findings indicated that CRLF1 may be required for ZBTB7A-induced activation of AKT signaling. Collectively, these results identified CRLF1 as a functional downstream effector of ZBTB7A and highlighted that the oncogenic properties of ZBTB7A in OV are mediated, at least in part, through its regulation of CRLF1.

Discussion

OV remains a high-mortality malignancy characterized by late diagnosis, rapid intraperitoneal dissemination, marked molecular heterogeneity and frequent development of therapeutic resistance. These challenges highlight the need for new biological entry points beyond current strategies (2,5). Because TFs orchestrate the gene-expression states underlying proliferation, EMT and metastatic competence, delineating TF-centered circuits offers a plausible route to biomarkers and tractable downstream targets (31). In the current study, ZBTB7A was identified as a TF that was aberrantly upregulated in OV. Integrative analyses across independent patient cohorts demonstrated that elevated ZBTB7A expression was associated with a poor OS. Moreover, single-cell transcriptomic profiling revealed that ZBTB7A-high malignant cells were enriched for proliferative, migratory and EMT-related gene programs. Consistent with these transcriptomic features, gain and loss-of-function experiments revealed that ZBTB7A could promote cell viability, colony formation and migration, whereas ZBTB7A knockdown reduced these phenotypes. Mechanistically, ZBTB7A activated CRLF1 transcription, and CRLF1 silencing attenuated the ZBTB7A-driven increases in cell proliferation and migration. Collectively, these findings support a model in which a ZBTB7A/CRLF1 transcriptional axis promotes OV aggressiveness.

TFs serve a pivotal role in the oncogenic programs of OV, directing cellular identity, survival, proliferation and plasticity in response to intrinsic mutations and extrinsic environmental signals (8,9). Increasing evidence has indicated that OV cells rely on transcriptional regulators to maintain their malignant phenotypes and adapt to therapeutic stress. For example, paired box 8, a lineage-specific TF essential, is frequently amplified in high-grade serous OV, and regulates genes involved in metabolism and proliferation (16,32). Similarly, FOXM1 promotes G_2/M transition and genomic stability, and its upregulation is associated with poor survival and platinum resistance (33,34). Canonical EMT regulators such as SNAI1, TWIST1 and ZEB1 suppress epithelial markers, and facilitate dissemination and immune evasion (35-37). The findings of the present study revealed that ZBTB7A may act as an oncogenic TF, identifying it as an upstream regulator associated with poor clinical outcomes and aggressive

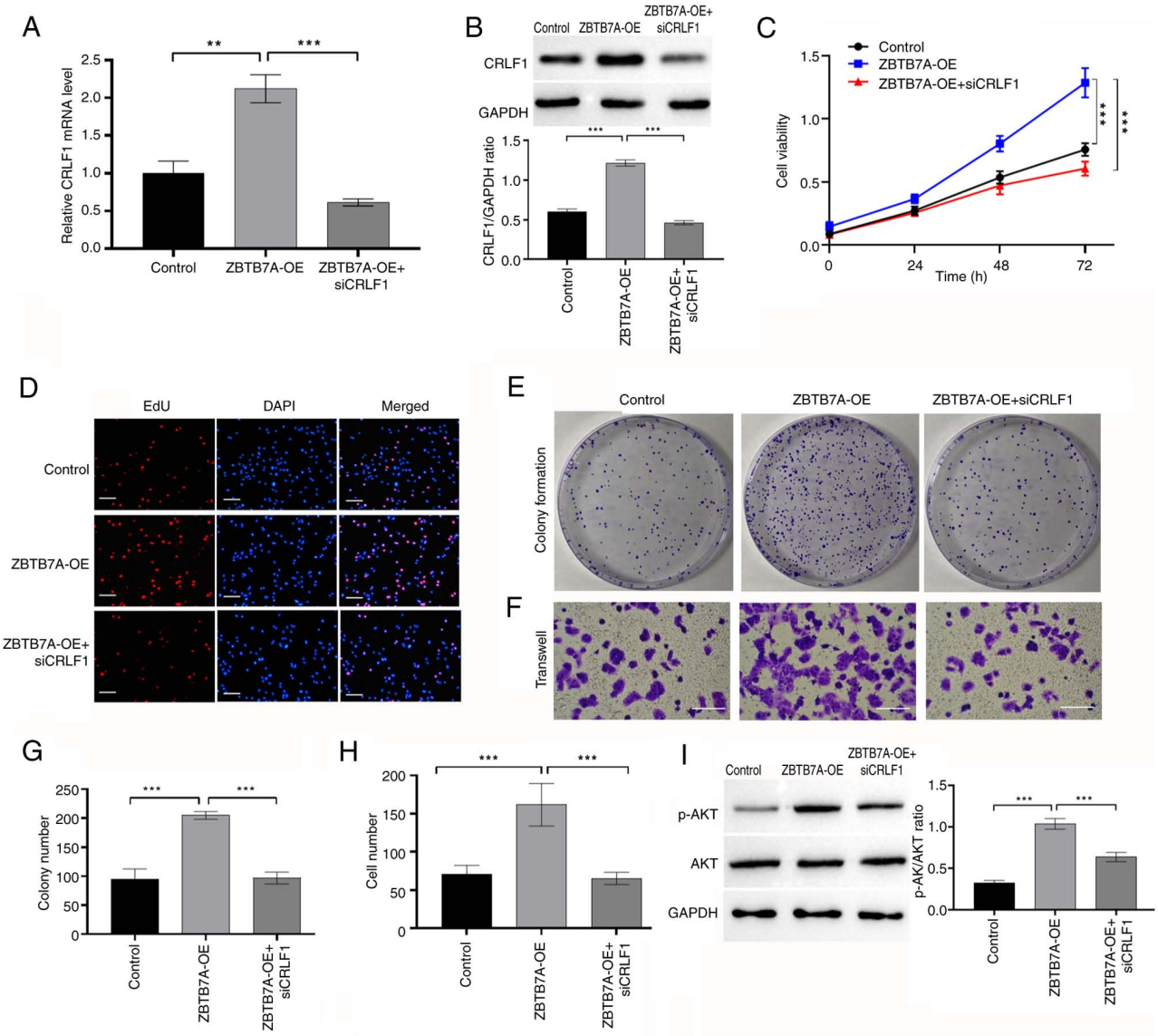

Figure 6. CRLF1 mediates ZBTB7A-induced oncogenic phenotypes. (A) Reverse transcription-quantitative PCR and (B) western blotting analyzed CRLF1 knockdown and ZBTB7A-OE. (C) Cell Counting Kit-8 assay showing rescue of proliferation after CRLF1 knockdown. (D) EdU assay showing impaired DNA synthesis. Scale bar, 100 μm. (E) Representative images of colony formation assays in the indicated groups. (F) Representative images of Transwell assays in the indicated groups. (G) Semi-quantification of colony numbers from three independent experiments. (H) Semi-quantification of cell numbers from three independent Transwell assay experiments. Scale bar, 50 μm. (I) Western blot analysis of p-AKT (Ser473) and total AKT in OVCAR3 cells. Representative blots are shown and semi-quantitative analysis of p-AKT normalized to total AKT is presented. Data are presented as the mean ± SD from three independent experiments. **P<0.01, ***P<0.001. CRLF1, cytokine receptor-like factor 1; OE, overexpression; p-, phosphorylated; si, small interfering; ZBTB7A, zinc finger and BTB domain-containing 7A.

cellular phenotypes. Unlike classical EMT TFs that function through direct suppression of epithelial genes such as cadherin-1, in the present study, ZBTB7A was shown to act as a transcriptional activator. The results revealed that it upregulated CRLF1, a secreted CRLF previously linked to pro-survival signaling in neuronal and fibrotic contexts (38). The oncogenic role of CRLF1 remains poorly characterized; however, emerging evidence suggests its involvement in activating the JAK-STAT, PI3K/AKT and MAPK/ERK signaling pathways, which are known to contribute to OV progression, stemness and chemoresistance (39,40). CRLF1 is a secreted glycoprotein that forms heterodimeric complexes, most notably with cardiotrophin-like cytokine factor 1, to activate gp130 and ciliary neurotrophic factor receptor signaling (41), ultimately engaging JAK-STAT, MAPK/ERK and PI3K/AKT pathways (40). These pathways are frequently hyperactivated in OV and contribute to key malignant properties such as cell survival, migration, stemness maintenance and resistance to chemotherapy. Although the role of CRLF1 in OV remains poorly characterized, emerging evidence suggests its involvement in activating the JAK-STAT, PI3K/AKT, and MAPK/ERK signaling pathways, prompting further investigation into its potential oncogenic function (40,42). To the best of our knowledge, the present study provided the first evidence that CRLF1 is transcriptionally induced by ZBTB7A and mediates key oncogenic outputs downstream of ZBTB7A. Silencing CRLF1 significantly impaired ZBTB7A-driven cell proliferation and motility, indicating that CRLF1 is not

merely a transcriptional target but a functionally important downstream effector. Given the role of CRLF1 in cytokine signaling, these findings suggest that ZBTB7A-driven CRLF1 expression may reinforce a tumor-promoting autocrine/paracrine microenvironment, allowing cancer cells to co-opt developmental cytokine circuits for malignant gain.

Despite these insights, the present study has several limitations. First, although it was demonstrated that ZBTB7A transcriptionally activates CRLF1 and that CRLF1 contributes to downstream oncogenic function, the precise downstream signaling pathways through which CRLF1 exerts these effects remain incompletely elucidated. Second, the *in vitro* assays provided mechanistic insights into the role of the ZBTB7A/CRLF1 axis in promoting OV cell proliferation and migration; however, the absence of an *in vivo* study limits the full assessment of its functional relevance in the native tumor microenvironment. Future studies will therefore focus on *in vivo* validation of the ZBTB7A/CRLF1 axis. These will include OV xenograft models using cells with stable ZBTB7A-OE or knockdown and/or CRLF1 silencing to assess tumor growth, tumor burden and survival outcomes. In addition, orthotopic or intraperitoneal implantation models will be employed to better recapitulate OV dissemination and ascites formation. Third, the broader clinical applicability of ZBTB7A or CRLF1 as biomarkers or therapeutic targets requires further evaluation in larger, well-annotated patient cohorts and diverse preclinical models. In addition, the survival analyses were strengthened by providing HR and 95% CI values, and multivariate Cox regression models adjusted for key clinical variables (age and tumor grade), which confirmed that ZBTB7A and CRLF1 may be independent predictors of poor OS in TCGA-OV. However, the unavailability of tumor stage information was acknowledged in the pan-cancer dataset used, which represents a limitation of the prognostic analysis.

In conclusion, the current study identified ZBTB7A as a clinically relevant TF that drives OV aggressiveness through transcriptional activation of CRLF1. Through integrative analyses spanning patient data, single-cell mapping and functional experiments, the results revealed that the ZBTB7A/CRLF1 axis may not only be associated with poor prognosis, but could also mechanistically contribute to tumor growth and migration. These findings underscore the importance of transcriptional networks in shaping malignant phenotypes and raise the possibility that CRLF1 or its downstream signaling components may serve as novel therapeutic entry points.

Acknowledgements

Not applicable.

Funding

No funding was received.

Availability of data and materials

The data generated in the present study may be requested from the corresponding author.

Authors' contributions

XH conceptualized the present study, performed the experiments, analyzed the data and wrote the original draft. YC conceptualized the present study, and reviewed and edited the manuscript. XH and YC confirm the authenticity of all the raw data. Both authors read and approved the final manuscript.

Ethics approval and consent to participate

Not applicable.

Patient consent for publication

Not applicable.

Competing interests

The authors declare that they have no competing interests.

References

1. Wang L, Zhang Q, Wang X, Dong Z, Liu S, Wang Q, Zhang Z and Xing J: Therapeutic landscape of ovarian cancer: Recent advances and emerging therapies. Biomark Res 13: 103, 2025.
2. Shah M, Chen TY, Ison G, Fiero MH, Zhang H, Gao X, Neilson M, Goldberg KB, Nair A, Ricks TK, *et al*: Overall survival and the evolving benefit-risk assessment for poly (ADP-ribose) polymerase inhibitors in advanced ovarian cancer. J Clin Oncol 43: 2218-2227, 2025.
3. Aggarwal R, Sheikh A, Akhtar M, Ghazwani M, Hani U, Sahebkar A and Kesharwani P: Understanding gold nanoparticles and their attributes in ovarian cancer therapy, Mol Cancer 24: 88, 2025.
4. Wu C, Chen D, Stout MB, Wu M and Wang S: Hallmarks of ovarian aging. Trends Endocrinol Metab 36: 418-439, 2025.
5. Gupta R, Kumar R, Penn CA and Wajapeyee N: Immune evasion in ovarian cancer: Implications for immunotherapy and emerging treatments. Trends Immunol 46: 166-181, 2025.
6. Wang Z, Liu Y and Yang Q: Navigating PARP inhibitor resistance in ovarian cancer: Bridging mechanistic insights to clinical translation. Curr Treat Options Oncol 26: 797-819, 2025.
7. Therachiyil L, Bhat AA and Uddin S: Claudins in ovarian cancer: Emerging biomarkers and therapeutic targets. Tissue Barriers: Aug 13, 2025 (Epub ahead of print).
8. Wang Y, He S, Huang Q, Yang J, Yang C and Ding J: The roles of YY1 in reproductive system: an overview. Chem Biol Interact 417: 111560, 2025.
9. Liu J, Wang H, Wan H, Yang J, Gao L, Wang Z, Zhang X, Han W, Peng J, Yang L and Hong L: NEK6 dampens FOXO3 nuclear translocation to stabilize C-MYC and promotes subsequent de novo purine synthesis to support ovarian cancer chemoresistance. Cell Death Dis 15: 661, 2024.
10. Wu A, Li S, Feng C, He R, Wu R, Hu Z, Huang J, Wang W, Huang L and Qiu L: Fn14 Controls the SIRT2-Mediated deacetylation of slug to inhibit the metastasis of epithelial ovarian cancer. Adv Sci (Weinh) 12: e2501552, 2025.
11. Zhao F, Liu G, Xiong L, Yao L, Wang L and Zhang Z: Effect of sufentanil on the proliferation, apoptosis, and epithelial-mesenchymal transition of ovarian cancer cells by regulating the SMAD3/SNAIL signaling pathway. J Mol Histol 56: 99, 2025.
12. Vikramdeo KS, Miree O, Anand S, Sharma A, Srivastava SK, Singh S, Rocconi RP and Singh AP: MYB/AKT3 axis is a key driver of ovarian cancer growth, aggressiveness, and chemoresistance. J Ovarian Res 18: 179, 2025.
13. Fu Z, Chen K, Zheng F, Gong W, Chao D and Lu C: FCGBP promotes ovarian cancer progression via activation of IL-6/JAK-STAT signaling pathway. J Transl Med 23: 827, 2025.
14. Lin J, Liu H, Fukumoto T, Zundell J, Yan Q, Tang CA, Wu S, Zhou W, Guo D, Karakashev S, *et al*: Targeting the IRE1α/XBP1s pathway suppresses CARM1-expressing ovarian cancer. Nat Commun 12: 5321, 2021.

15. Hasan A, Khan NA, Uddin S, Khan AQ and Steinhoff M: Deregulated transcription factors in the emerging cancer hallmarks. Semin Cancer Biol 98: 31-50, 2024.
16. Bleu M, Mermet-Meillon F, Apfel V, Barys L, Holzer L, Bachmann Salvy M, Lopes R, Amorim Monteiro Barbosa I, Delmas C, Hinniger A, *et al*: PAX8 and MECOM are interaction partners driving ovarian cancer. Nat Commun 12: 2442, 2021.
17. Cheng Q, Li L and Yu M: Construction and validation of a transcription factors-based prognostic signature for ovarian cancer. J Ovarian Res 15: 29, 2022.
18. Nameki RA, Chang H, Yu P, Abbasi F, Lin X, Reddy J, Haro M, Fonseca MA, Freedman ML, Drapkin R, *et al*: Rewiring of master transcription factor cistromes during high-grade serous ovarian cancer development. bioRxiv: Apr 12, 2023 (Epub ahead of print).
19. Xiang X, Mao J, Tang D, Huang H and Tang H: The ZBTB family in cardiac development and diseases. Biochem Biophys Res Commun 771: 152026, 2025.
20. Zhou Y, Chen X and Zu X: ZBTB7A as a therapeutic target for cancer. Biochem Biophys Res Commun 736: 150888, 2024.
21. Gupta S, Singh AK, Prajapati KS, Kushwaha PP, Shuaib M and Kumar S: Emerging role of ZBTB7A as an oncogenic driver and transcriptional repressor. Cancer Lett 483: 22-34, 2020.
22. Maeda T, Hobbs RM and Pandolfi PP: The transcription factor Pokemon: A new key player in cancer pathogenesis. Cancer Res 65: 8575-8578, 2005.
23. Yue R, Chen Y, Lai W and Wei W: miR-106b exerts tumor suppressive functions in ovarian carcinoma by directly targeting ZBTB7A. Minerva Med 112: 657-658, 2021.
24. Bonome T, Levine DA, Shih J, Randonovich M, Pise-Masison CA, Bogomolniy F, Ozbun L, Brady J, Barrett JC, Boyd J and Birrer MJ: A gene signature predicting for survival in suboptimally debulked patients with ovarian cancer. Cancer Res 68: 5478-5486, 2008.
25. Arend RC, Scalise CB, Gordon ER, Davis AM, Foxall ME, Johnston BE, Crossman DK and Cooper SJ: Metabolic alterations and WNT signaling impact immune response in HGSOC. Clin Cancer Res 28: 1433-1445, 2022.
26. Zhang Z, Zhan Q, Eckert M, Zhu A, Chryplewicz A, De Jesus DF, Ren D, Kulkarni RN, Lengyel E, He C and Chen M: RADAR: Differential analysis of MeRIP-seq data with a random effect model. Genome Biol 20: 294, 2019.
27. Geistlinger L, Oh S, Ramos M, Schiffer L, LaRue RS, Henzler CM, Munro SA, Daughters C, Nelson AC, Winterhoff BJ, *et al*: Multiomic analysis of subtype evolution and heterogeneity in high-grade serous ovarian carcinoma. Cancer Res 80: 4335-4345, 2020.
28. Livak KJ and Schmittgen TD: Analysis of relative gene expression data using real-time quantitative PCR and the 2(-Delta Delta C(T)) Method. Methods 25: 402-408, 2001.
29. Zhou Q, Tang H, Wang Y, Hua Y, Ouyang X and Li L: Hyperoside mitigates PCOS-associated adipogenesis and insulin resistance by regulating NCOA2-mediated PPAR-γ ubiquitination and degradation. Life Sci 364: 123417, 2025.
30. Wang S, Wang C, Hu Y, Li X, Jin S, Liu O, Gou R, Zhuang Y, Guo Q, Nie X, *et al*: ZNF703 promotes tumor progression in ovarian cancer by interacting with HE4 and epigenetically regulating PEA15. J Exp Clin Cancer Res 39: 264, 2020.
31. Du G, Huang X, Su P, Yang Y, Chen S, Huang T and Zhang N: The role of SOX transcription factors in prostate cancer: Focusing on SOX2. Genes Dis 12: 101692, 2025.
32. Luo Y, Liu X, Chen Y, Tang Q, He C, Ding X, Hu J, Cai Z, Li X, Qiao H and Zou Z: Targeting PAX8 sensitizes ovarian cancer cells to ferroptosis by inhibiting glutathione synthesis. Apoptosis 29: 1499-1514, 2024.
33. Liu C, Barger CJ and Karpf AR: FOXM1: A multifunctional oncoprotein and emerging therapeutic target in ovarian cancer. Cancers (Basel) 13: 3065, 2021.
34. Battistini C, Kenny HA, Zambuto M, Nieddu V, Melocchi V, Decio A, Lo Riso P, Villa CE, Gatto A, Ghioni M, *et al*: Tumor microenvironment-induced FOXM1 regulates ovarian cancer stemness. Cell Death Dis 15: 370, 2024.
35. Taki M, Abiko K, Baba T, Hamanishi J, Yamaguchi K, Murakami R, Yamanoi K, Horikawa N, Hosoe Y, Nakamura E, *et al*: Snail promotes ovarian cancer progression by recruiting myeloid-derived suppressor cells via CXCR2 ligand upregulation. Nat Commun 9: 1685, 2018.
36. Liu J, Shu G, Wu A, Zhang X, Zhou Z, Alvero AB, Mor G and Yin G: TWIST1 induces proteasomal degradation of beta-catenin during the differentiation of ovarian cancer stem-like cells. Sci Rep 12: 15650, 2022.
37. Sestito R, Tocci P, Roman C, Di Castro V and Bagnato A: Functional interaction between endothelin-1 and ZEB1/YAP signaling regulates cellular plasticity and metastasis in high-grade serous ovarian cancer. J Exp Clin Cancer Res 41: 157, 2022.
38. Looyenga BD, Resau J and MacKeigan JP: Cytokine receptor-like factor 1 (CRLF1) protects against 6-hydroxydopamine toxicity independent of the gp130/JAK signaling pathway. PLoS One 8: e66548, 2013.
39. Pasquin S, Laplante V, Kouadri S, Milasan A, Mayer G, Tormo AJ, Savin V, Sharma M, Martel C and Gauchat JF: Cardiotrophin-like cytokine increases macrophage-foam cell transition, J Immunol 201: 2462-2471, 2018.
40. Yu ST, Zhong Q, Chen RH, Han P, Li SB, Zhang H, Yuan L, Xia TL, Zeng MS and Huang XM: CRLF1 promotes malignant phenotypes of papillary thyroid carcinoma by activating the MAPK/ERK and PI3K/AKT pathways. Cell Death Dis 9: 371, 2018.
41. Crisponi L, Buers I and Rutsch F: CRLF1 and CLCF1 in development, health and disease. Int J Mol Sci 23: 992, 2022.
42. Yu ST, Sun BH, Ge JN, Shi JL, Zhu MS, Wei ZG, Li TT, Zhang ZC, Chen WS and Lei ST: CRLF1-MYH9 interaction regulates proliferation and metastasis of papillary thyroid carcinoma through the ERK/ETV4 axis. Front Endocrinol (Lausanne) 11: 535, 2020.